J. Fluid Mech. (1971), *vol.* 47, *part* 4, *pp.* 737–764
Printed in Great Britain

Magneto-fluid-mechanic pipe flow in a transverse magnetic field. Part 1. Isothermal flow

By R. A. GARDNER† AND P. S. LYKOUDIS
School of Aeronautics, Astronautics and Engineering Sciences,
Purdue University, West Lafayette, Indiana

(Received 5 May 1970)

An experimental investigation was conducted in a circular pipe to examine the influence of a transverse magnetic field on the structure of turbulent shear flow of a conducting fluid (mercury). In the present paper, part 1, mean velocity profiles, turbulence intensity profiles, velocity fluctuation spectra, axial pressure drop profiles, and skin friction data are presented which quantitatively exhibit the Hartmann effect and damping of the velocity fluctuations over a broad range of Reynolds numbers and magnetic fields. The results of heat transfer experiments will be reported by the authors in the following paper, part 2.

1. Introduction

The experimental study of the interaction of magnetic fields with conducting fluids most likely has its origin in Faraday's (1832) imaginative attempt to measure the flow of the river Thames using underwater electrodes and the earth's weak magnetic field. The era of practical research, however, was not initiated until more than a century later with the pioneering works of Hartmann & Lazarus (1937*b*) in which they investigated isothermal laminar flow of mercury through electrically insulated channels placed in a transverse magnetic field. Hartmann & Lazarus's (1937*a*) theoretical results showed that the field flattens the velocity profile as a result of its interaction with the induced electric current (the so-called 'Hartmann effect') and from Hartmann & Lazarus's (1937*b*) experimental skin friction data it was inferred that the magnetic field acts directly to damp out or at least inhibit the velocity fluctuations of turbulent flow. The existence of the Hartmann and fluctuation damping effects has been confirmed by direct measurement in recent experiments. Branover & Lielausis (1965) and Brouillette & Lykoudis (1967) demonstrated the Hartmann effect with velocity profiles measured in rectangular channels in a transverse magnetic field; and Branover, Slyusarev & Shcherbinin (1965) and Hua (1968) experimentally verified the existence of the turbulence suppression effect in similar channel experiments. It should also be noted that Fraim & Heiser (1968) observed the fluctuation damping

† Present address: Mechanical and Aerospace Engineering Department, Washington University, St Louis, Missouri

effect qualitatively in their recent experiments in a circular pipe in an axial magnetic field, and Sajben & Fay (1967) measured the damping effect in a jet flow in an axial field.

Very little quantitative information of this nature is available for pipe flow in a transverse magnetic field. The first experiments by Shercliff (1956), Khozhainov (1966), and Ihara, Tajima & Matsushima (1967) produced skin friction measurements, but they were limited to low Reynolds numbers. Recently, Loeffler, Maciulaitis & Hoff (1969) reported skin friction and velocity profile data in transverse fields at much higher Reynolds numbers. Their velocity profile data exhibited the Hartmann flattening along 0° from the field and also showed that the profiles become more rounded in the wall region at 90°. Only zero and very high magnetic field data were reported.

It is the objective of the present investigation to fill in the gaps in the available data and to present new data on various aspects of the flow so that we might begin to understand the overall picture of turbulent magneto-fluid-mechanic (MFM) shear flow in a transverse field.

Reynolds number	10^4–10^6
Average velocity	$\frac{1}{10}$–10 ft/sec
Electromagnet	
Rectangular pole faces	12 in. × 50 in.
Air gap	3 in.
Magnetic field	0–13 000 gauss
Skin friction test section	
Length	122.9 in.
Diameter	1·364 in.
Total L/d	90
Magnetic L/d	37
Velocity profile test section	
Entrance section length	43·9 in.
Test section length	79·0 in.
Diameter	1.431 in.
Magnetic L/d	35
Temperature	70 °F

TABLE 1. Characteristic parameters

2. Experimental system

A closed-loop system was constructed to accommodate three independent investigations in a transverse magnetic field: pipe flow (the present work), channel flow by Hua (1968) and natural convection by Papailiou & Lykoudis (1968). The general layout of the apparatus is shown in figure 1, and figure 2 is a sketch showing the orientation of the transverse field. A list of general operating conditions is given in table 1.

All parts of the loop in contact with the mercury were fabricated from stainless steel, Teflon, plexiglass, or nylon in order to prevent corrosion or contamination.

A complete description of the individual components of the loop is given by Gardner (1969).

A large water-cooled d.c. electromagnet with 12 in. × 50 in. pole faces was mounted on a movable carriage so that it could traverse the distance between the pipe and channel experiments. The magnet also had the capability of rotating 360° about a horizontal axis through its centre of gravity and was used with its pole faces vertical for the natural convection experiment located in the centre of the loop.

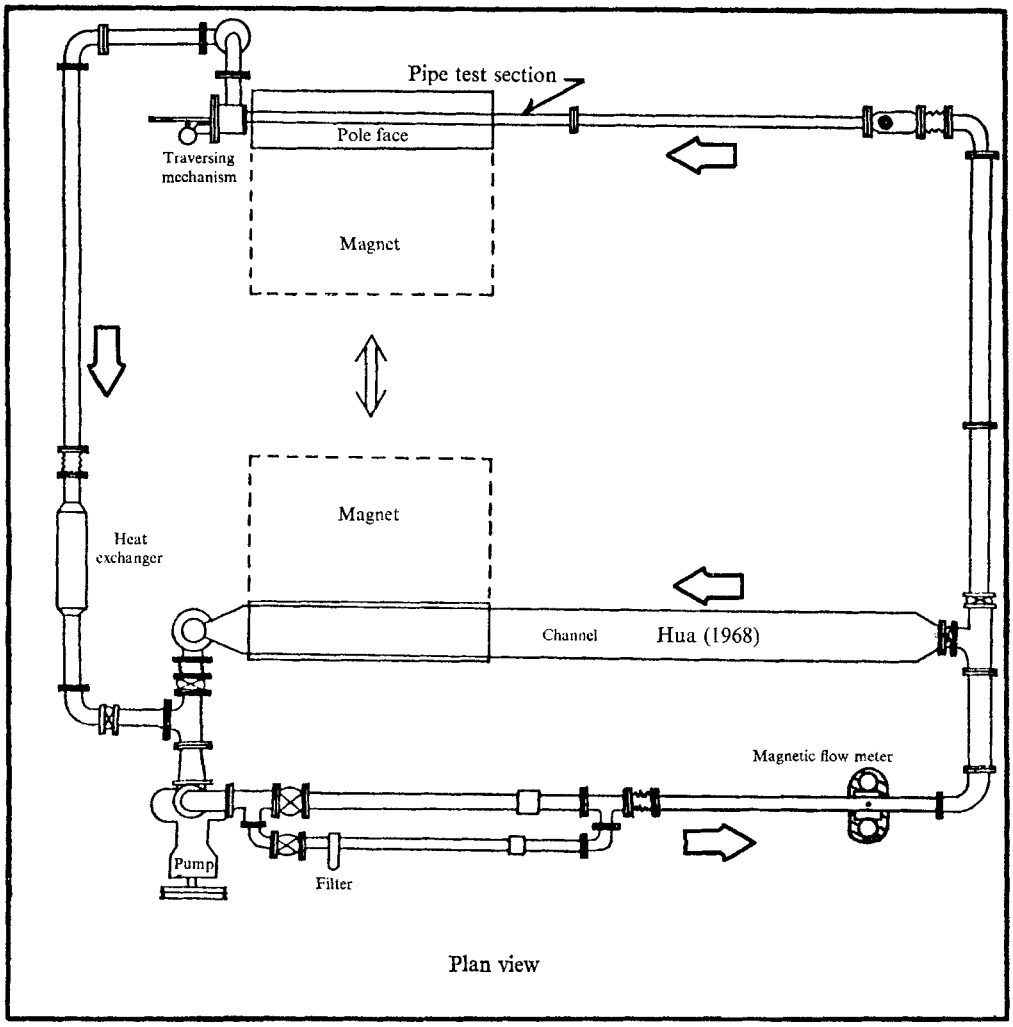

FIGURE 1. General diagram of MFM loop.

Mercury was circulated around the loop by the centrifugal pump located in the lower left-hand corner of figure 1. Downstream of the pump was a parallel section of one and two inch piping, each having a valve for flow control. A filter unit was installed after the valve in the smaller line to remove oxide and other contaminants from the mercury. Just upstream of the test section area the flow

went through the bulk mixing-cup chamber in which several baffles and screens mixed the flow.

The mercury flowed through the test section, traversing mechanism, mixing baffles and outlet bulk mixing-cup chamber, a flexible bellows, and a heat exchanger (tube and shell type) before returning to the pump to be recirculated.

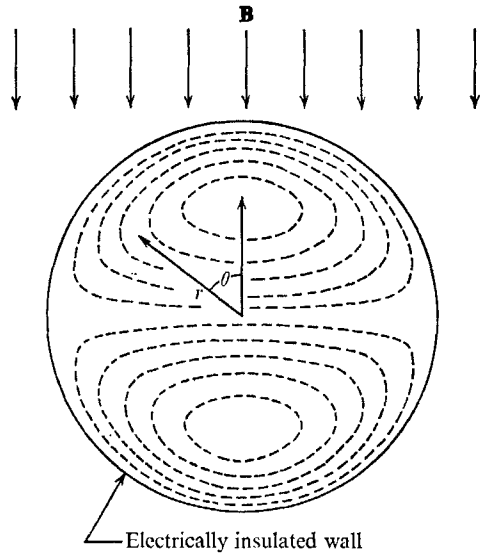

FIGURE 2. Pipe cross-section showing co-ordinate system, orientation of the magnetic field, and induced electric current loops. Radial co-ordinate, r, is normalized by the pipe radius. **B** is the transverse magnetic field; ----, induced current loops ($\bar{J}$).

Preliminary experiments indicated that the 30 h.p. motor furnished with the pump caused vibrations which propagated into the test section area even though that portion of the loop was mechanically isolated from the pump by three flexible bellows. Two steps were taken to eliminate this problem. A smaller three h.p. pump motor was isolated from the pump frame by a system of pulleys and belts and several additional diagonal braces were added to the loop structure. These improvements minimized the vibrations and raised the natural frequencies of the loop structure. The loop was run at Reynolds numbers up to 350000 with the small motor. The 30 h.p. motor was used at higher Reynolds numbers. Gardner (1969) discusses the influence of the mechanical vibrations in more detail. In general, they were not found to be significant. Two test sections were used in the course of this investigation and are described below.

The skin friction test section

This test section was made from seamless, heavy wall, 316 stainless steel pipe. The inside of the pipe near the ends was reamed to correct the 'necking in' that occurred when the entrance and exit flanges were welded to the pipe. Thirteen static pressure taps were installed by drilling $\frac{1}{32}$ in. holes through the wall and heli-arc welding a $\frac{1}{4}$ in. pipe nipple (their ends were milled to fit the curvature of the pipe) over the small hole. Then the inside of the pipe was polished to a shiny finish.

In order to simplify the nature of the skin friction data and allow comparison with existing data, it was necessary to insulate electrically the inside of the pipe by coating the 60 in. of the pipe in the magnetic field with a 0·001 in. of FEP Teflon.

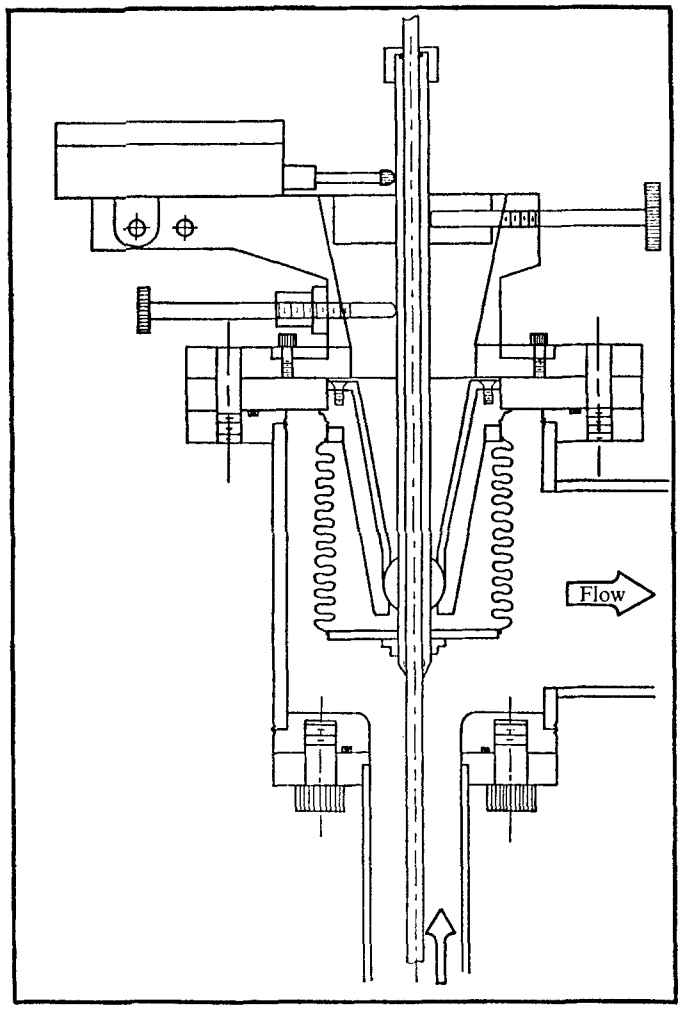

FIGURE 3. Probe traversing mechanism.

The velocity profile test section

This test section was made from welded 316 stainless-steel tubing. (Welded tubing was chosen over the seamless variety because it had a more uniform wall thickness. This was desirable as this test section was also to be used in the heat transfer experiments reported in part 2 (Gardner & Lykoudis 1971).) Flanges were welded on both ends and the inside of the pipe was carefully reamed and polished. Then a 0·001 in. coating of FEP Teflon was sprayed on the inside surface to insulate electrically the pipe from the flow. Except for a scratch line from the pipe weld (probably 0.001 in. or 0.002 in. deep), the inside of the pipe was a smooth round surface.

A traversing mechanism, shown in figure 3, was located in the exit of the test section in order to probe the velocity field. The probe holder was mounted in a ball joint so that it could move the tip of any type of probe with a 0.250 in. shank to a selected position inside the pipe. The radial co-ordinate was measured with a 2-inch dial gauge and the angular co-ordinate with a protractor scale.

The average flow rate was measured by a magnetic flow meter which was constructed in the form of an aluminium channel with a thin plexiglass liner cemented to the inside walls. Two electrodes were mounted flush with the upper and lower walls and a large permanent magnet (4 in. × 4 in. pole faces, 3100 gauss, $2\frac{1}{2}$ in. gap) was used with its field perpendicular to the flow and electrodes. This flow meter was calibrated by measuring the average velocity in the test section with a Pitot-static tube. The precision to which one could set the flow rate was better than $\pm 1\,\%$.

A Vidar 520 integrating digital volt meter was used to measure the flow meter's signal and all other d.c. measurements (magnet shunt, thermocouples, etc.). Velocity profile and fluctuation data were measured with a Thermo-Systems 1050 constant-temperature hot-film anemometer and a Thermo-Systems 1060 true r.m.s. meter. (The 1060 meter could make r.m.s. measurements down to 0·1 cycle/sec.) The spectral measurements were recorded by a Panoramic analyzer.

3. Mean velocity and turbulence profile measurements

Preliminary discussion

Isothermal mean velocity and axial fluctuation intensity profiles were measured with a constant temperature hot-film anemometer. The orientation of the axis of the sensor was always perpendicular to both the radial and axial directions.

A constant fluid temperature was maintained by adjusting a small flow of cold water through the heat exchanger to remove the heat generated by the pump and viscous dissipation. Maintaining isothermal flow was important because the hot-film anemometer was found to be very sensitive to the free stream temperature. (A change of 1° F would change the indicated mean velocity by about 20%!) At each measurement the temperature was measured (in either the inlet or outlet mixing-cup) and all data were corrected for small deviations from the temperature at which the calibration curves were taken. In addition, the r.m.s. value of the axial fluctuation intensity was corrected for the anemometer noise at zero flow.

In order to measure the bridge voltage of the anemometer more accurately, it was averaged by the integrating digital volt meter over a period of about thirty seconds. The r.m.s. value of the axial velocity fluctuation was measured simultaneously with the mean velocity with either the 30 or 100 second time constant on the Thermo-Systems 1060 r.m.s. meter. The long averaging time was necessary at low flow rates when the frequencies are low.

Several different types of hot-film probes were used, but most of the measurements were made with a standard 6 mil probe. In preliminary measurements it was observed that the magnetic field interacted with the vortex shedding behind the sensor. This caused an apparent angular dependence at the centre of the pipe with a large relative error in the r.m.s. value as the turbulence was damped

by the magnetic field. Filling in the area between the fingers of the probe with an epoxy eliminated this problem. A parabolic or wedge type of probe could also have been used. Gardner (1969) discusses the magnetic interaction with the vortex shedding in more detail.

A low overheat of 1·07 was used in order to prolong probe life, and the probe was always kept in the mercury in order to keep it clean. After the first 75 h of use, the calibration curves were reproducible and the probe was used for another 209 h of active service without failure. The initial unstable period was probably due to the formation of an oxide impurity layer on the probe. When it was finally removed from the mercury it was found to be uniformly wetted.

It was also observed in these first experiments that the magnetic field had an influence on the free convection that develops about the probe. At zero velocity the bridge voltage had an immediate drop when the field was turned on, indicating that the free convection in the vicinity of the probe was being inhibited. This drop in bridge voltage was dependent on the angular orientation of the probe relative to the magnetic field. In later experiments, with characteristic flow speeds of 1 ft/sec, this angular dependence was not found except at very high magnetic fields. Only data which are free of this natural convection effect (no angular dependence at a point) will be reported.

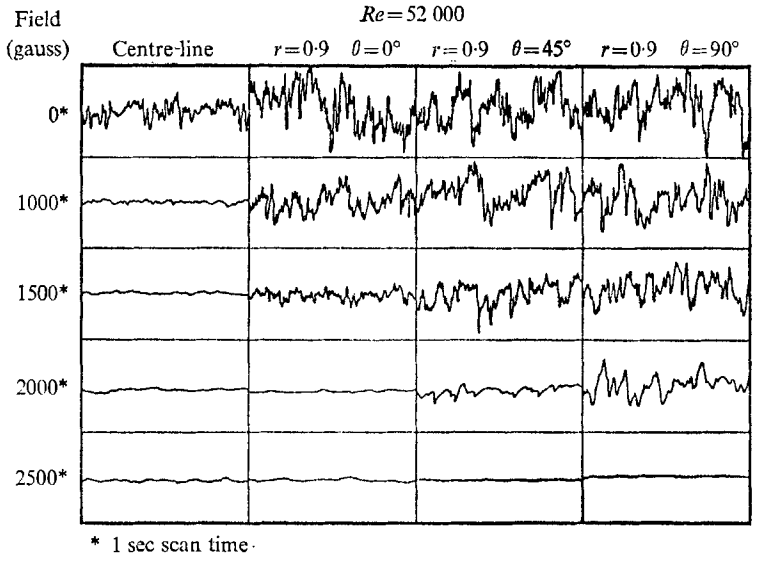

FIGURE 4. Turbulent velocity signal, Re = 52000.

A qualitative study (oscilloscope photographs) of the influence of the magnetic field on the velocity fluctuations was made at three Reynolds numbers (10000; 52000; 157000) in order to gain some insight into the character of the flow. Figure 4 shows that the centre-line fluctuations are damped out first and an angular dependence appears as the field increases. The fluctuations at $\theta = 90°$ from the vertical field are the last to be damped out. Figures 5 and 6 are pictures that were taken when the flow was in the transition region just before it became

'laminar'. Note that the low Reynolds number data of figure 5 show that the fluctuations are intermittent at 90° near the wall. On the other hand, no intermittency was observed at the higher Reynolds number, figure 6. When the field was increased past the value shown in these figures, the turbulence was damped out throughout the cross-section of the pipe.

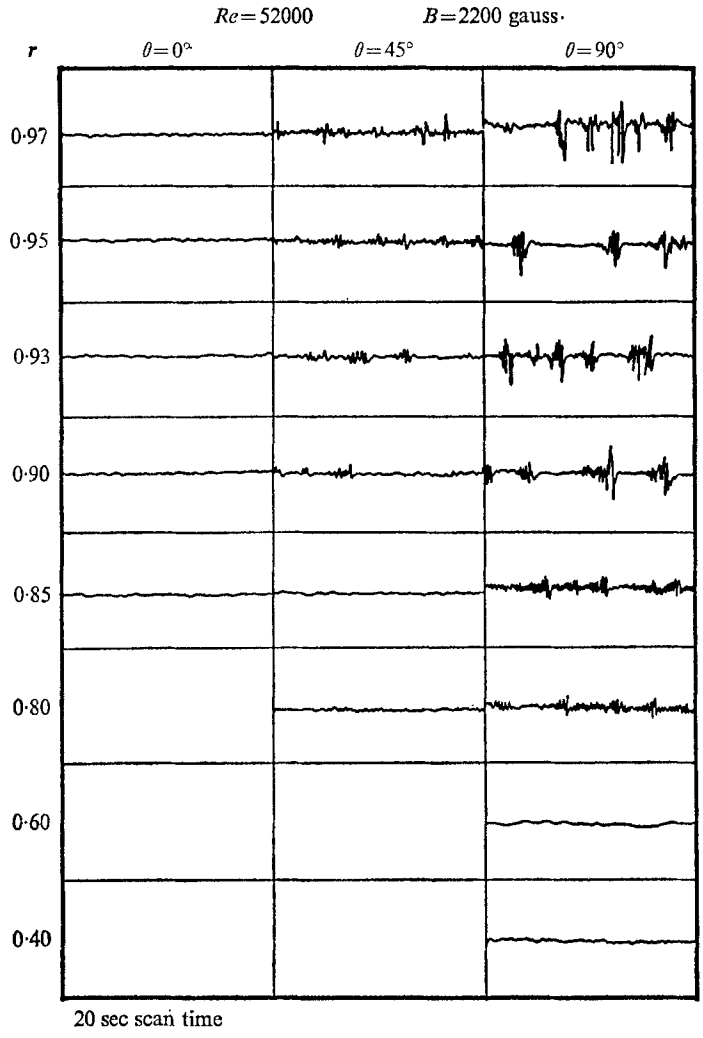

FIGURE 5. Turbulent velocity signal, Re = 52000, B = 2200 gauss, flow near transition.

Velocity profiles

The zero-field velocity profile data for the three Reynolds numbers investigated are shown in figure 7. The data are plotted in the universal co-ordinates to show that the profiles follow the expected logarithmic distribution.† The zero-field

† The universal co-ordinates u^* and y^* are defined in the following manner:

$$u^* = U/(\tau_w/\rho)^{\frac{1}{2}} \quad \text{and} \quad y^* = ay(\tau_w/\rho)^{\frac{1}{2}}/\nu.$$

Here U, τ_w, ρ, a, ν, and y are the local velocity, shear at the wall, density, pipe radius, kinematic viscosity and distance from the wall normalized by the pipe radius.

velocity fluctuation data shown in figure 8 are compared to Laufer's (1951) data taken in air. They coincide except in the centre of the flow where the present experimental data indicate a higher turbulence intensity. This could be due to the experimental probe and/or other experimental apparatus.

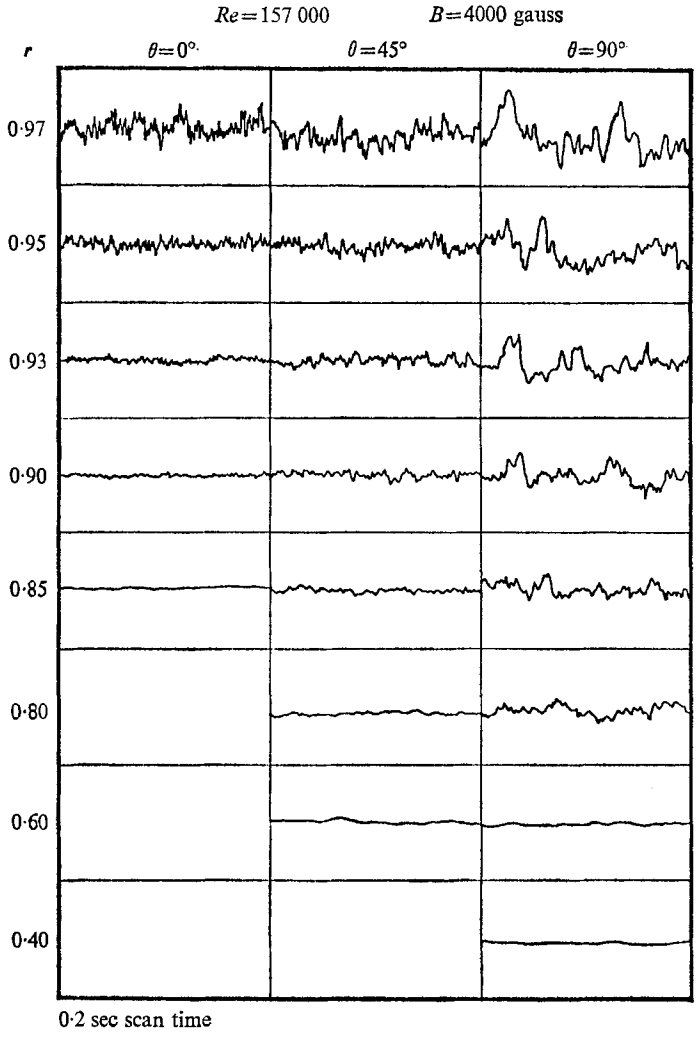

FIGURE 6. Turbulent velocity signal, Re = 157 000, B = 4000 gauss, flow near transition.

Figure 9 shows the MFM velocity profile data at three angles (0°, 45°, 90°) and two Reynolds numbers. Along 0° from the vertical magnetic field the profiles flatten (Hartmann effect) as the field increases. The normalized profiles at 45° increase near the wall and show a trend to increase then decrease slightly in the central portion of the profile as the field increases. Along 90° the profiles become more rounded with lower shear at the wall. For all three angles the centre-line velocity decreased about 10 % at the maximum field.

In the last stage of the adjustment of the velocity profile along 90°, when the intermittency appeared, the local velocity near the wall increased when a turbulent burst was recorded. This indicates that, in the last stage of adjustment, the profile 'flips' to the laminar MFM profile in a discontinuous way at 90° near the wall. The instability of the velocity profile was not found in the near-wall areas at 45° and 0°. This was probably due to the fact that the Hartmann flattening along 0° has eliminated the gradient in the velocity profile (and hence the source from which turbulence can be sustained): whereas, along 90°, the gradient in the velocity profile was increased in a good portion of the flow. Velocity fluctuation data also gave a similar indication of the instability of this region at 90°.

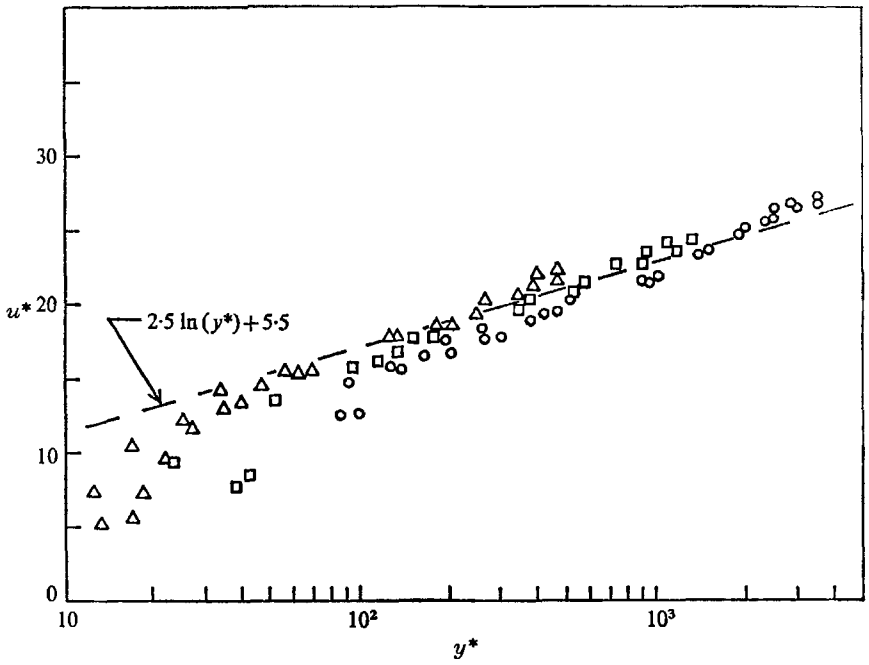

FIGURE 7. Universal velocity distribution of zero-field velocity profile data. *Re*: △, 16000; □, 52100; ○, 157000.

Velocity fluctuation intensity profiles are shown in figures 10 and 11. (u_x' is the axial r.m.s. velocity fluctuation, non-dimensionalized by the average velocity.) The fluctuations are damped out strongly in the centre of the flow and then as the magnetic field was increased an angular dependence appears. The intermittent fluctuations at $\theta = 90°$ are the last ones to be damped out. The MFM velocity fluctuation intensity is plotted against the ratio of Hartmann number to Reynolds number, M/Re, at four positions in the flow in figures 12 and 13.† The $\theta = 90°$, $r = 0{\cdot}9$ data show an abrupt drop in the transition region where the intermittency appears and the final adjustment of the mean velocity profile takes place.

† Both M and Re are based on the diameter of the pipe as a characteristic length. $M = Bd(\sigma/\mu)^{\frac{1}{2}}$, $Re = \rho U_m d/\mu$.

Several attempts were made to correlate the velocity fluctuations at the centre of the pipe with the various non-dimensional parameters of the flow. It was found that the normalized experimental data (for small magnetic fields) could be correlated with an exponential function of $M^2/Re^{0.75}$. This correlation is shown in figure 14. (Note that a semi-log plot is used so that an exponential form plots as a straight line.)

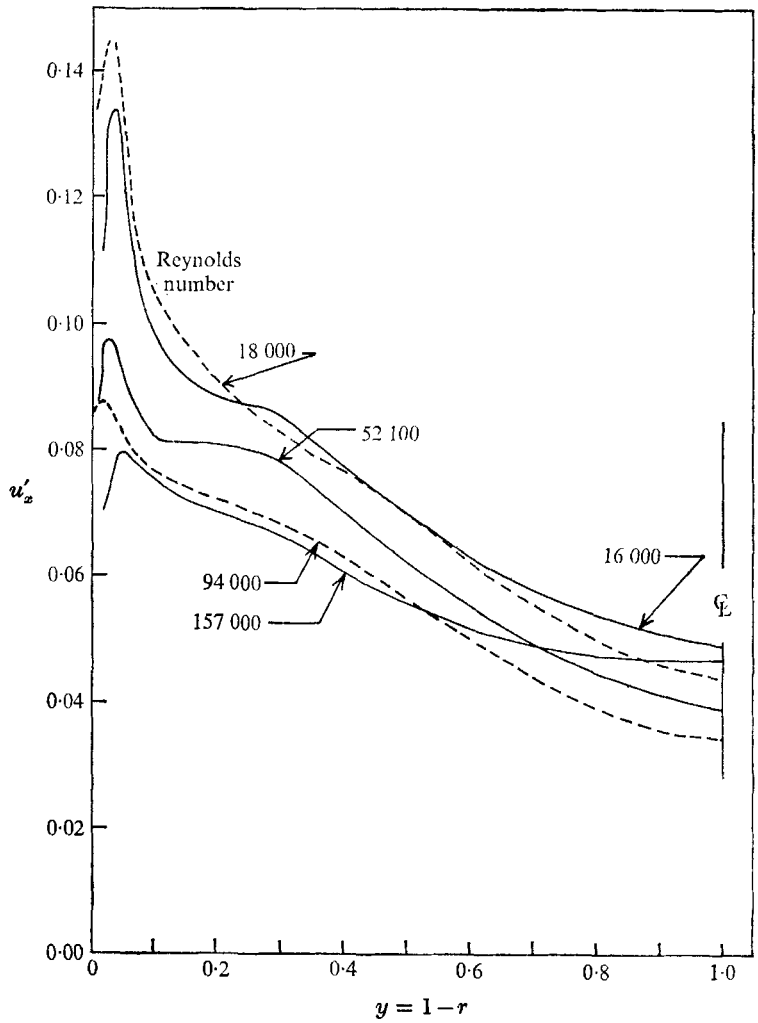

FIGURE 8. Zero-field velocity fluctuation intensity data. u'_x is non-dimensionalized by the average velocity. – – –, Laufer (1951); ——, present work.

In figure 14 the points of abrupt change in the slope of the data correspond to the values of the ratio M/Re where the angular dependence appears in the $r = 0{\cdot}9$ turbulence intensity data of figures 12 and 13. This indicates that the constant in the exponential form changes when the fluctuations near the wall are inhibited and the flow takes on an angular dependence.

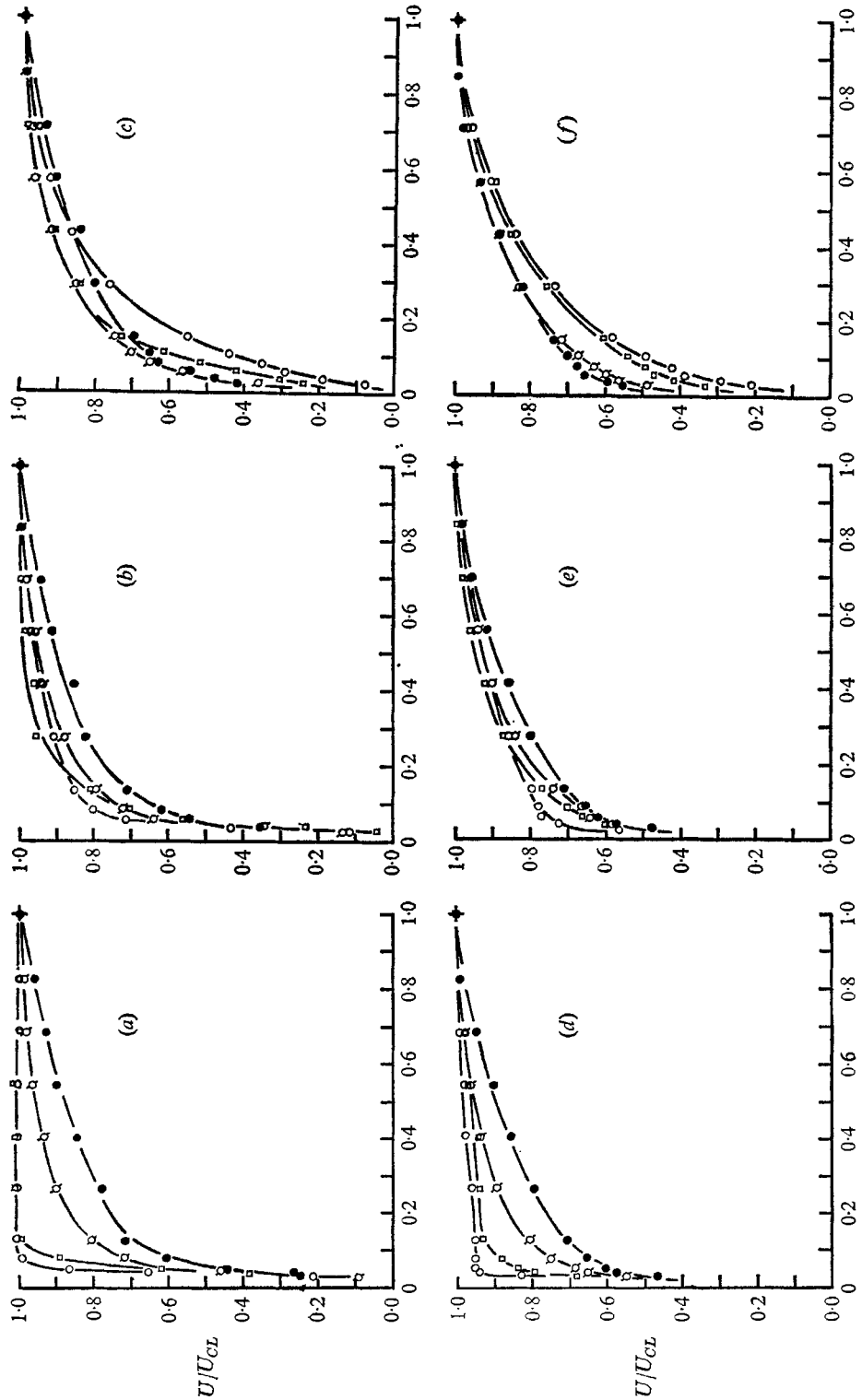

FIGURE 9. MFM velocity profiles for $\theta = 0°$, 45°, and 90° at $Re = 16000$ and 157000. (*a*) $Re = 16000$, 0° from field B (gauss): ●, 0; ◔, 500; □, 750; ○, 1500. (*b*) $Re = 16000$, 45° from field. B (gauss): ●, 0; ◔, 500; □, 750; ○, 1500. (*c*) $Re = 16000$, 90° from field. B (gauss): ●, 0; ◔, 500; □, 750; ○, 1500. (*d*) $Re = 157000$, 0° from field. B (gauss); ●, 0; ◔, 1500; □, 3000; ○, 5000. (*e*) $Re = 157000$, 45° from field. B (gauss): ●, 0; ◔, 1500; □, 3000; ○, 5000. (*f*) $Re = 157000$, 90° from field. B (gauss): ●, 0; ◔, 1500; □, 3000; ○, 5000.

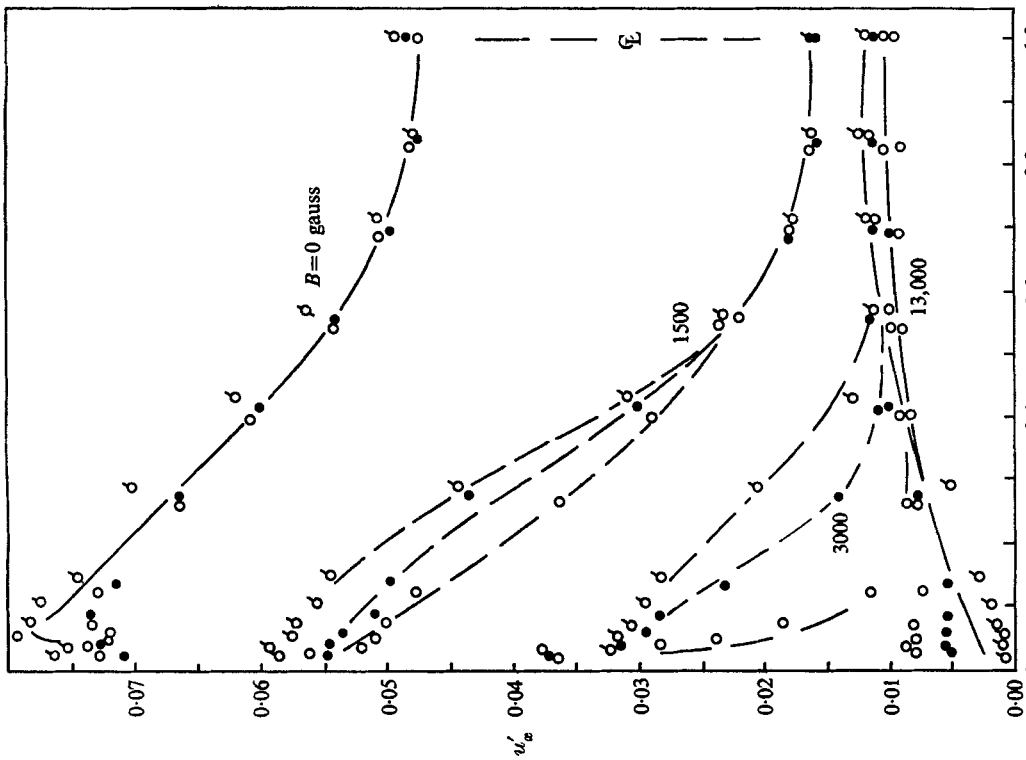

FIGURE 11. MFM velocity fluctuation intensity profiles, $Re = 157\,000$. Angle from field: ○, 0°; ●, 45°; ◌, 90°.

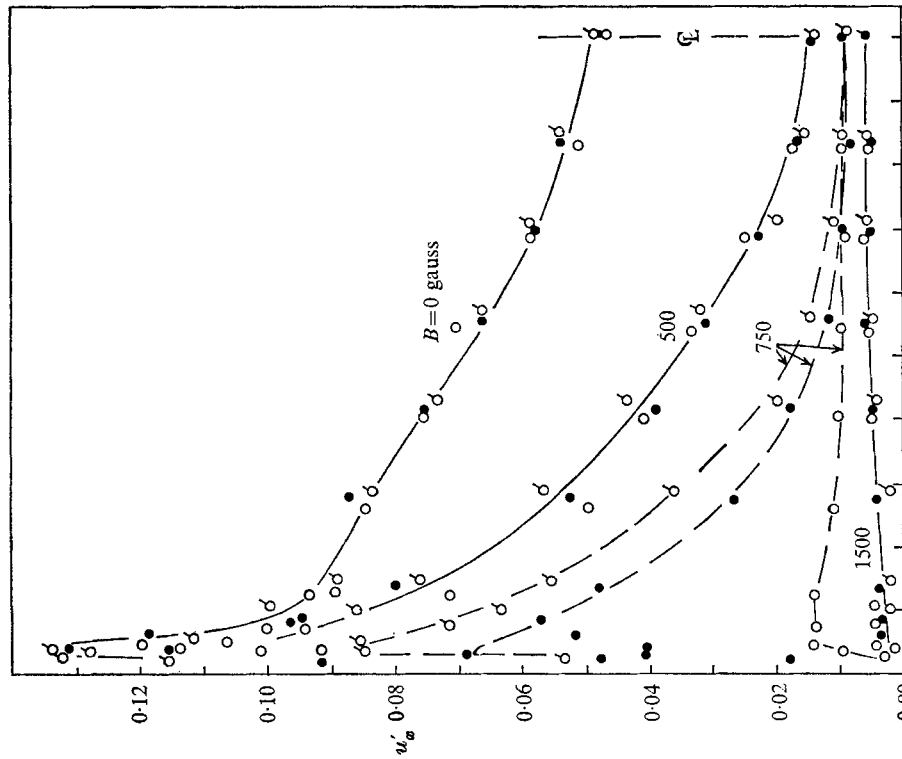

FIGURE 10. MFM velocity fluctuation intensity profiles, $Re = 16\,000$. Angle from field: ○, 0°; ●, 45°; ◌, 90°.

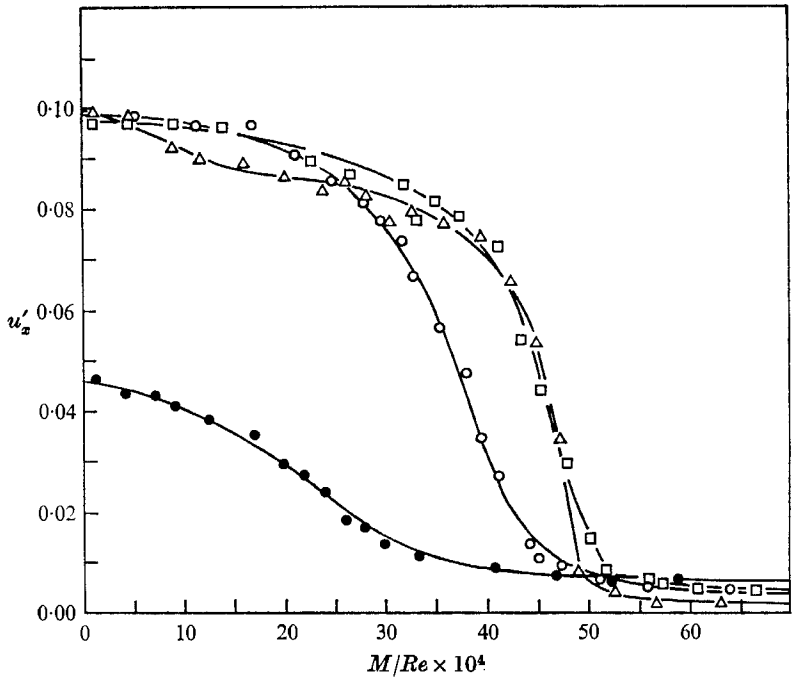

FIGURE 12. MFM velocity fluctuation intensity *vs.* $M/Re \times 10^4$, $Re = 16000$. ●, centre-line; ○, $r = 0{\cdot}9$, $\theta = 0°$; □, $r = 0{\cdot}9$, $\theta = 45°$; △, $r = 0{\cdot}9$, $\theta = 90°$.

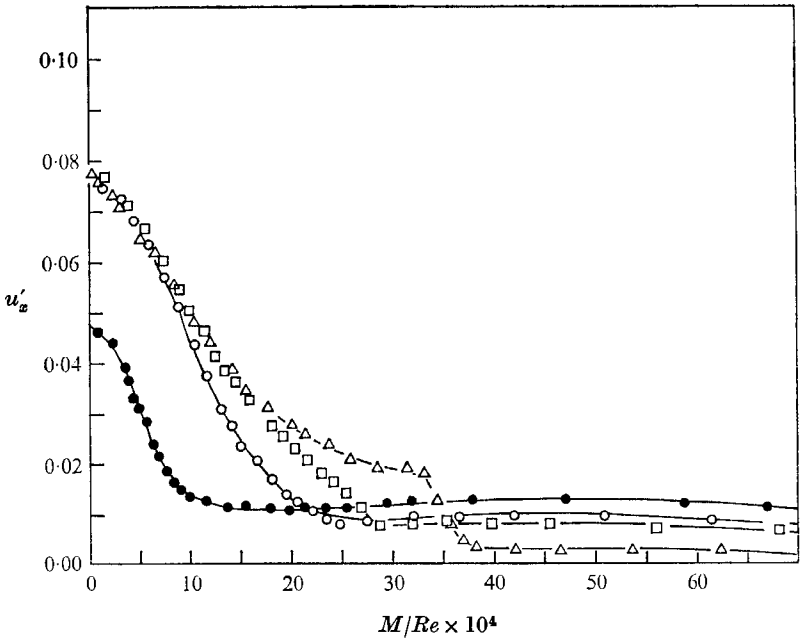

FIGURE 13. MFM velocity fluctuation intensity *vs.* $M/Re \times 10^4$, $Re = 157000$. See figure 12 for symbols.

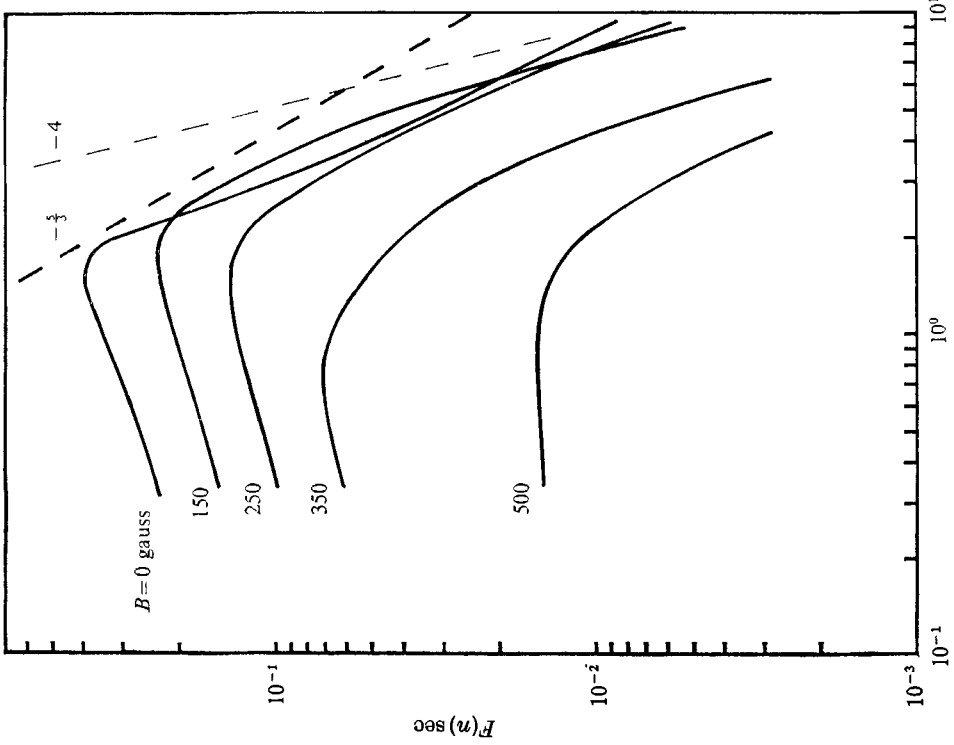

FIGURE 15. Axial velocity fluctuation spectra: $Re = 10\,300$, centre-line.

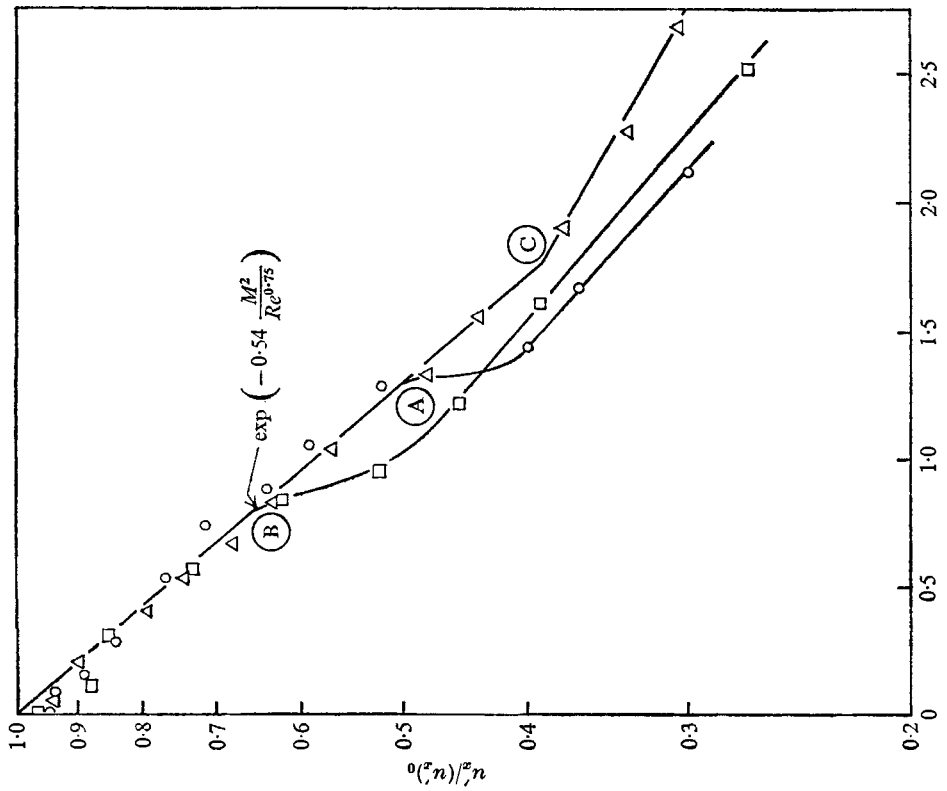

FIGURE 14. Correlation of centre-line velocity fluctuation data, normalized by the zero-field data. ○, $Re_1 = 16\,000$; □, $Re_2 = 52\,100$; △, $Re_3 = 157\,000$. Value of M/Re where slope changes: ○, $M/Re_1 = 26 \times 10^{-4}$; ⓑ, $M/Re_2 = 10 \times 10^{-4}$; ○, $M/Re_3 = 7{\cdot}5 \times 10^{-4}$.

Hua (1968), in a rectangular channel in a transverse field, found that his centre-line data showed a preference for the parameter M^2/Re. One would expect that this is the more desirable parameter since it is the ratio of the typical ponderomotive force to the typical inertia force. The data of the present experiment, however, show a definite preference for $M^2/Re^{0.75}$ indicating some influence of the viscous forces. Further experiments over a wider range of Reynolds numbers are now being conducted at the MFM Laboratory of Purdue University in order to substantiate the form of the damping correlation.

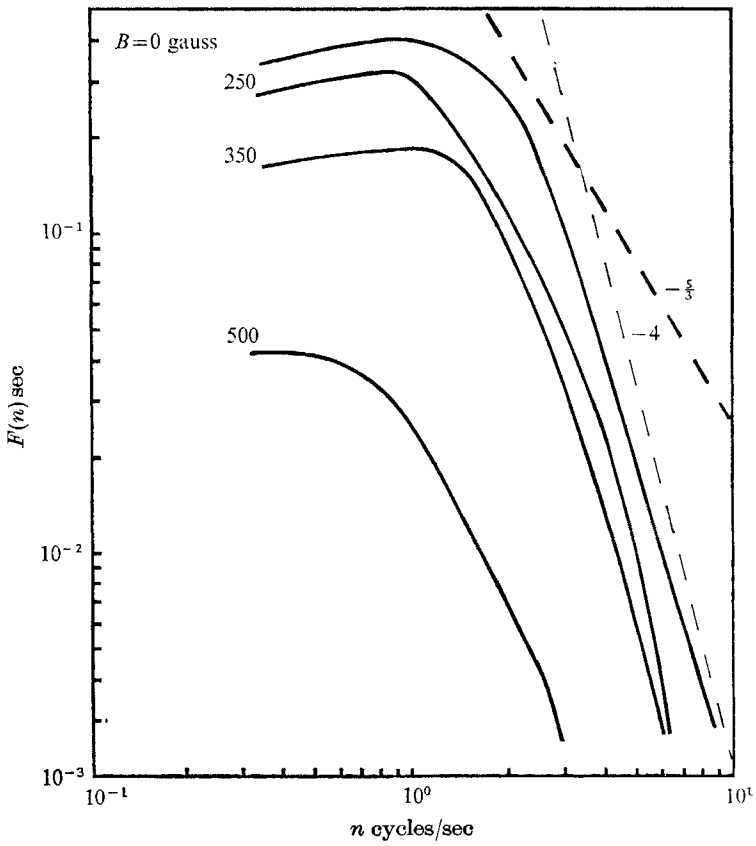

FIGURE 16. Axial velocity fluctuation spectra: $Re = 10300$, $r = 0{\cdot}9$, $\theta = 45°$.

4. Spectral measurements

The one-dimensional Taylor spectral density of the axial velocity fluctuation, $F(n)$, was measured by a Panoramic spectrum analyzer. The raw data of the analyzer was normalized by the area under the zero-field curve so that

$$\int_0^\infty F(n)\,dn = (u_x')^2/(u_x')^2_{B=0}. \tag{1}$$

A smooth curve was drawn through the data in the normalization process in order to reduce the data from analog to digital form for computational purposes.

The data were also corrected for the change in the sensitivity of the anemometer as the local velocity changed due to the influence of the magnetic field.

Three Reynolds numbers were investigated at four positions in the flow: on the centre-line; and at $r = 0.9$ for $\theta = 0°$, 45°, and 90°. Representative sets of these data in figures 15–19 show that the magnetic field damps all frequencies. The bulk of the energy is found in the low frequency range, and for $Re = 52\,100$ and 157 000, an inertial subrange is apparent where local isotropy exists and $F(n) \approx n^{-\frac{5}{3}}$. Figure 20 is a qualitative picture of the spectra in the high frequency range.

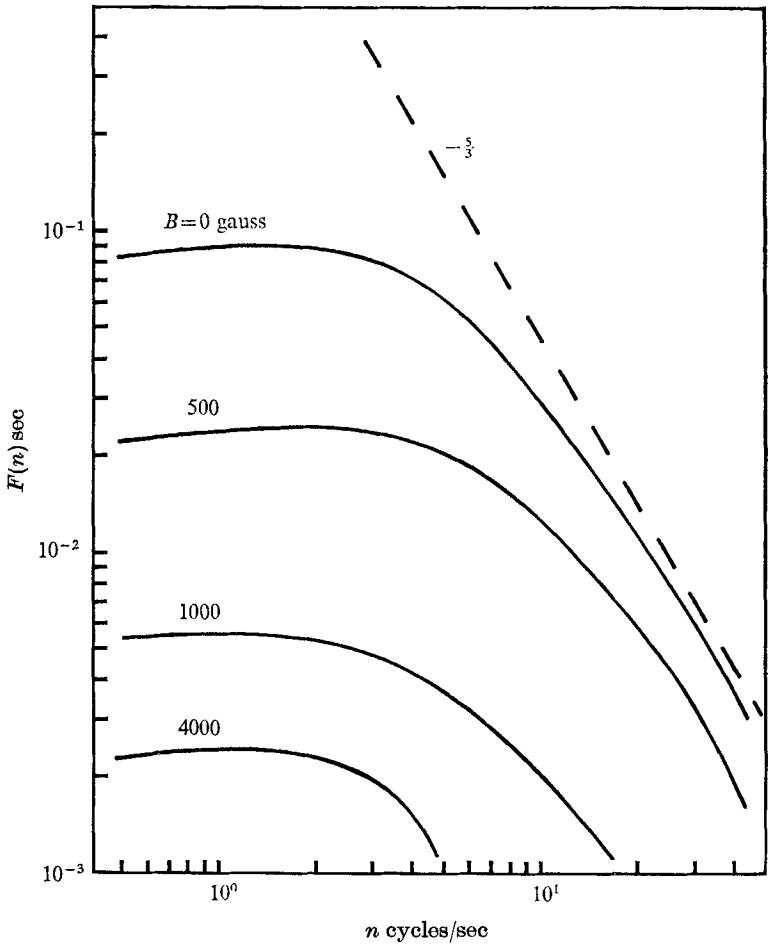

FIGURE 17. Axial velocity fluctuation spectra: $Re = 52\,100$, centre-line.

The spectra data for *small magnetic fields* show a weak tendency for the low frequencies to be damped more than the high frequencies. Then, when the magnetic field is made large enough to cause transition to the 'laminar' type of flow, the spectrum shifts to the low frequencies. These trends are more clearly shown on the linear plots of figures 21 and 22 where the spectra are plotted as a function of

wave-number, $k = 2\pi n/U_{\text{local}}$. Here, the spectra, $E(k)$, were normalized by their individual areas instead of the area under the zero-field spectrum.

A similar preferential damping of the low frequencies was reported recently by Blum *et al.* (1967) in their measurements of temperature fluctuations in a heated channel in a transverse magnetic field.

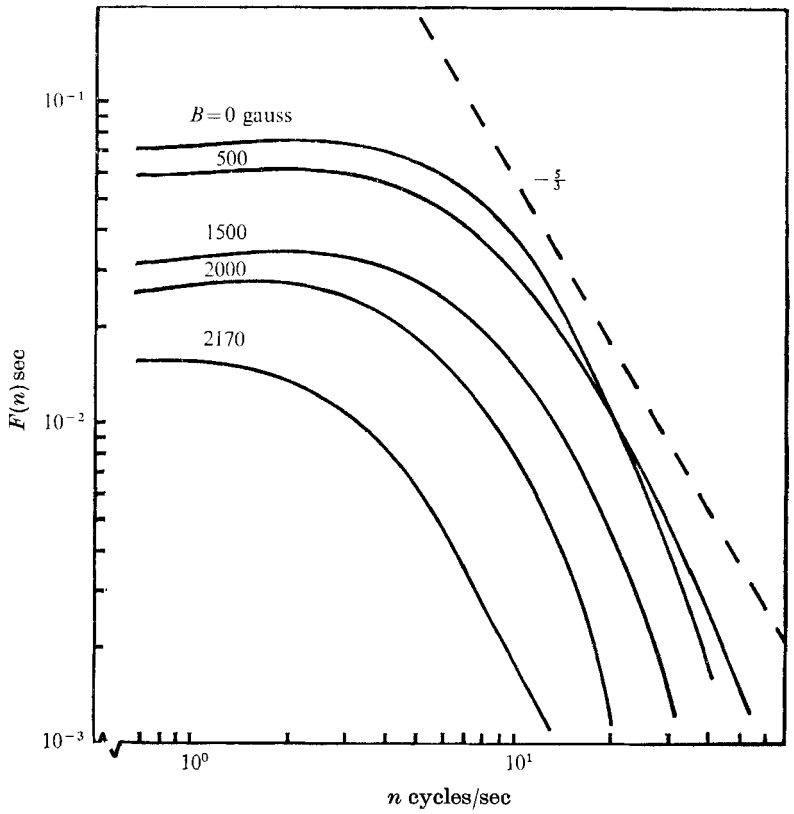

FIGURE 18. Axial velocity fluctuation spectra: $Re = 52100$, $r = 0{\cdot}9$, $\theta = 90°$.

One can only speculate that this weak preferential damping is due to the three-dimensional complexity of the flow. Along a 0° diameter the mean velocity gradient decreases; along a 90° diameter it increases. Thus, the mean velocity profile acquires a gradient in the azimuthal direction which must cause an adjustment in the production, diffusion, and scale of the turbulent fluctuations.

At $Re = 157000$ (centre-line) an anomaly appeared in the data in that the $B = 5500$ gauss spectrum was higher than the $B = 3500$ spectrum. This is consistent with the turbulence intensity data of figure 13 where u_x' at the centre-line shows a slight increase when the transition from turbulent to laminar flow takes place. The source of this disturbance was not identified, but it is most likely due to pump vibrations or pressure fluctuations in the flow outside of the test section area which propagated into the test section area.

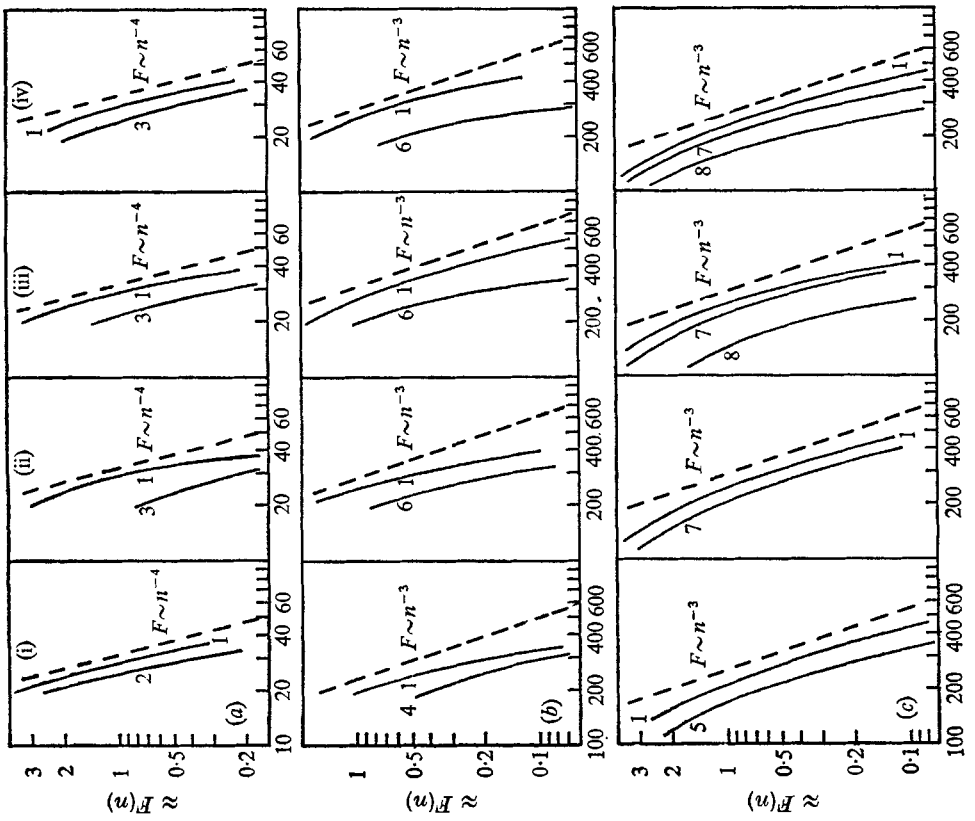

FIGURE 20. High frequency range of velocity fluctuation spectra. Row: (*a*) $Re = 10\,300$; (*b*) $Re = 52\,100$; (*c*) $Re = 157\,000$. Column: (i) centre-line; (ii) $r = 0{\cdot}9$, $\theta = 0°$; (iii) $r = 0{\cdot}9$, $\theta = 45°$; (iv) $r = 0{\cdot}9$, $\theta = 90°$. Curve: 1, $B = 0$ gauss; 2, $B = 150$ gauss; 3, $B = 350$ gauss; 4, $B = 500$ gauss; 5, $B = 800$ gauss; 6, $B = 1500$ gauss; 7, $B = 2000$ gauss; 8, $B = 3500$ gauss.

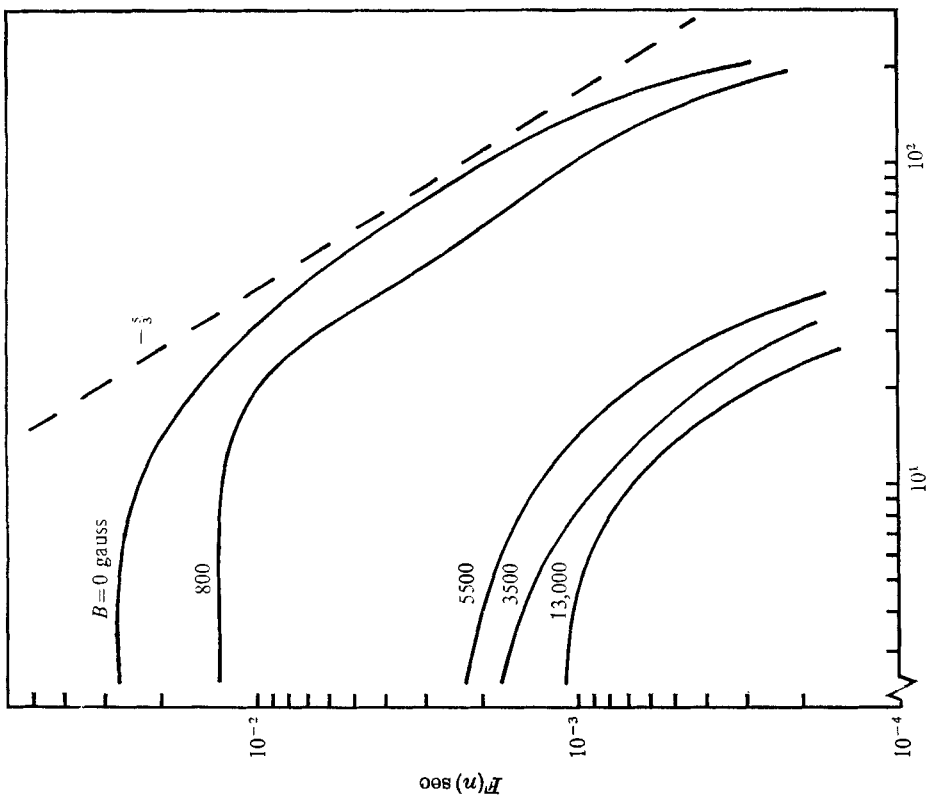

FIGURE 19. Axial velocity fluctuation spectra: $Re = 157\,000$, centre-line.

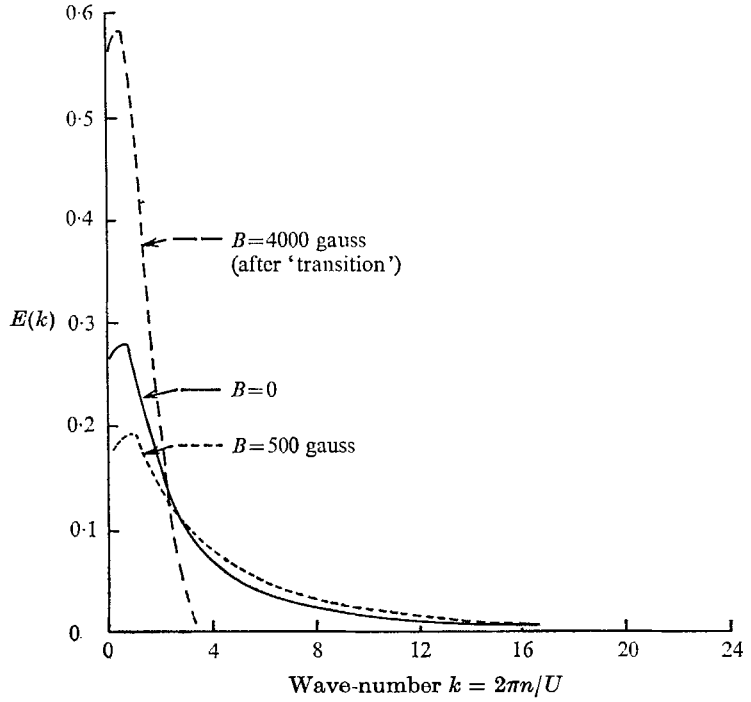

FIGURE 21. Linear plot of axial velocity fluctuation spectra: $Re = 52\,100$, centre-line. $E(k)$ was normalized such that $\int_0^\infty E(k)\,dk = 1{\cdot}0$.

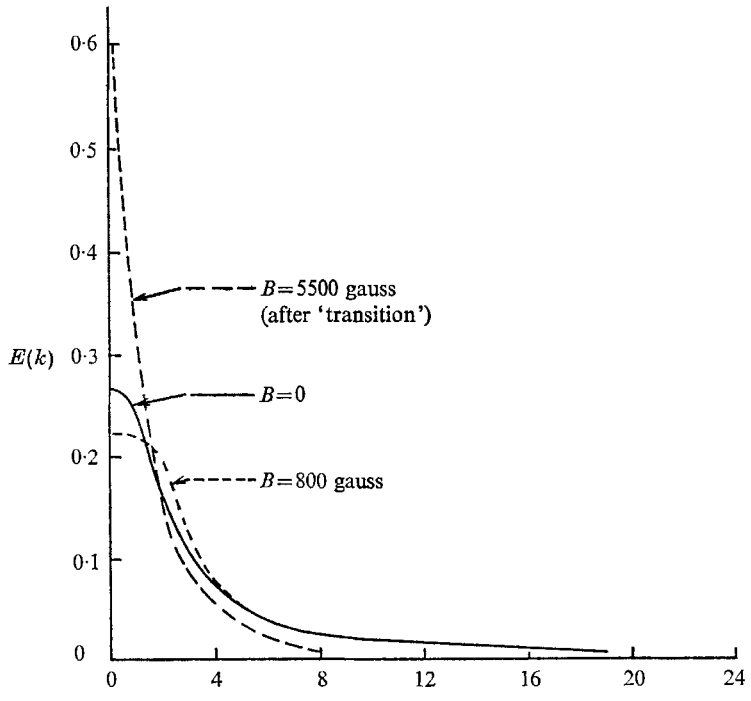

FIGURE 22. Linear plot of axial velocity fluctuation spectra: $Re = 157\,000$, centre-line. $E(k)$ was normalized such that $\int_0^\infty E(k)\,dk = 1{\cdot}0$.

5. Skin friction measurements

The axial pressure drop was measured between two pressure taps on the skin friction test section with both a micromanometer (accurate to $\pm 0{\cdot}001$ in. Hg) and a pressure transducer (accurate to $\pm 0{\cdot}00001$ in. Hg). The transducer was used in the measurement of small pressure differences characteristic of low Reynolds numbers. Although it was capable of measuring extremely small pressure differences, measurements below 0·0001 in. Hg were not reliable because this was of the same order of magnitude as the pressure fluctuations in the flow itself.

As was shown in figure 2, the electrically insulated wall forces the induced current to form closed loops, so there is no net ponderomotive force opposing the flow. The MFM skin friction coefficient can then be defined in the same manner as the zero field skin friction coefficient if we understand that $\bar{\tau}_w$ is now the circumferentially averaged wall shear stress. Then

$$C_f \equiv \bar{\tau}_w / \tfrac{1}{2}\rho U_m^2, \tag{2}$$

where ρ, and U_m are the density and average velocity.

Figures 23 and 24 are MFM pressure drop data taken at thirteen stations. Both entrance and exit effects are limited to a small region of a few diameters. Outside of the magnetic field, the slope of the data is the same as the $B = 0$ slope. Only at $Re = 450\,000$ and $B = 12\,500$ gauss does the flow show a significant magnetic entrance effect of about 10 diameters into the field.

After finding the region where the pressure gradient was a straight line, two taps were chosen in the linear portion and the complete set of MFM skin friction data were taken, figure 25. Both the micromanometer and the pressure transducer were used to take data at $Re = 50\,000$.

The data for constant Reynolds numbers were plotted against the ratio M/Re because C_f is a function of only M/Re for laminar flow. As M/Re increases, the data lose their Reynolds number dependence and follow the 'laminar line' because the turbulent fluctuations are being damped out and a transition from turbulent to 'laminar' flow takes place.

The dip in the skin friction data was first observed by Loeffler *et al.* (1969). Lacking information about the damping of the turbulent fluctuations, they gave a preliminary explanation that it was "probably due to a progressive transition or stabilization of the boundary layer". From the velocity profile and velocity fluctuation measurements in figures 9 to 13 it is easy to understand in more detail why this dip occurs. As M/Re increases, the velocity profile is adjusting from a turbulent axisymmetric profile to a profile which is flat along a 0° diameter and more rounded along a 90° diameter. Between values of $M/Re \times 10^4$ from 20 to 35 the final adjustment takes place rather abruptly as the turbulence is damped and transition takes place. This is analogous to the zero field skin friction data where a dip in the C_f data occurs in the transition region at about $Re = 2300$. (It should be noted that in figure 23 the $B = 7500$ and $B = 5000$ gauss data have the same slope because they are on opposite sides of this 'dip' region.)

A qualitative picture of the transition is shown in figure 26 where it can be seen that the 'dip' region coincides with the final damping of the fluctuations near the wall.

Transition data, figure 27, were taken by placing a hot-film anemometer probe in the region where the last fluctuations to be damped out occur ($\theta = 90°$, near the wall). A sharp decrease in the turbulence intensity was observed when the

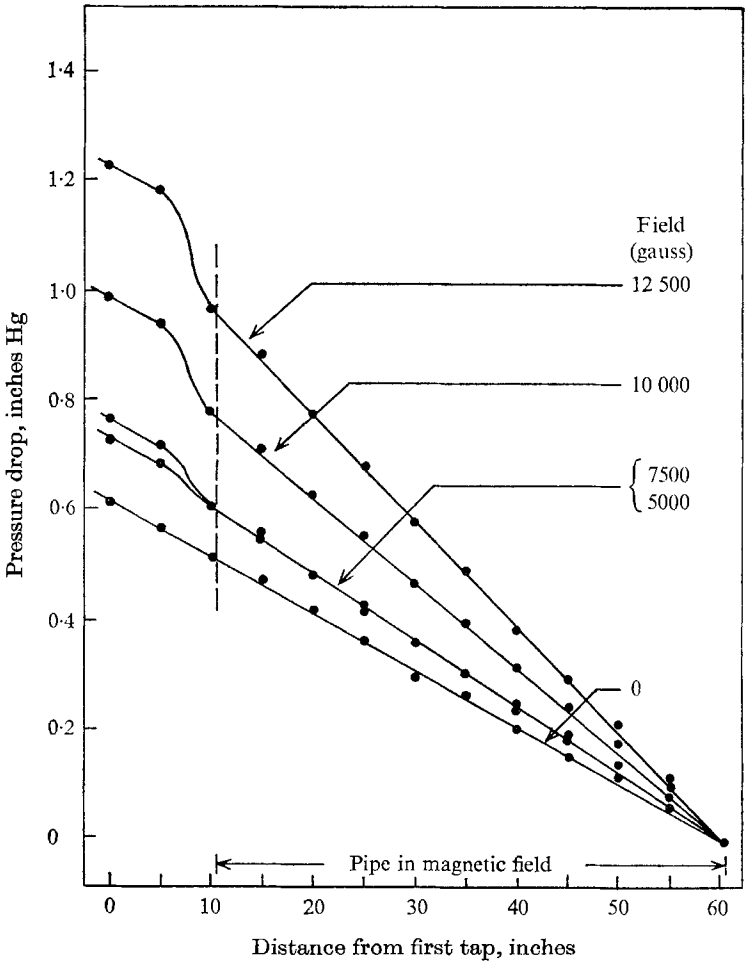

FIGURE 23. Pressure drop data, $Re = 200\,000$.

transition took place as the magnetic field was increased. This definition of transition is the minimum value of the ratio M/Re necessary to damp out all of the fluctuations. When the magnetic field was increased, giving higher values of M/Re, a 'laminar' flow resulted.

The data in figure 27 for transition from laminar to turbulent flow (the opposite kind of transition) were taken by slowly increasing the flow rate (Re), for a constant field, until fluctuations started to appear in the flow. The small difference between the two types of transition and the lack of large scatter in the

data are a strong indication that the transition point (from either direction) occurs at a predictable value of Hartmann number for a given Reynolds number. The 'critical' value of Reynolds number increases as the Hartmann number increases.

These transition data are important in understanding the skin friction data of figure 25 because they are additional evidence that the flow becomes a 'laminar' type of flow (with a sharp reduction in the fluctuations) when the skin friction data (at constant Reynolds number) intercept the so-called 'laminar line' derived by Shercliff (1956). The transition value of M/Re decreases as Reynolds number increases, and for high Reynolds numbers the transition point lies

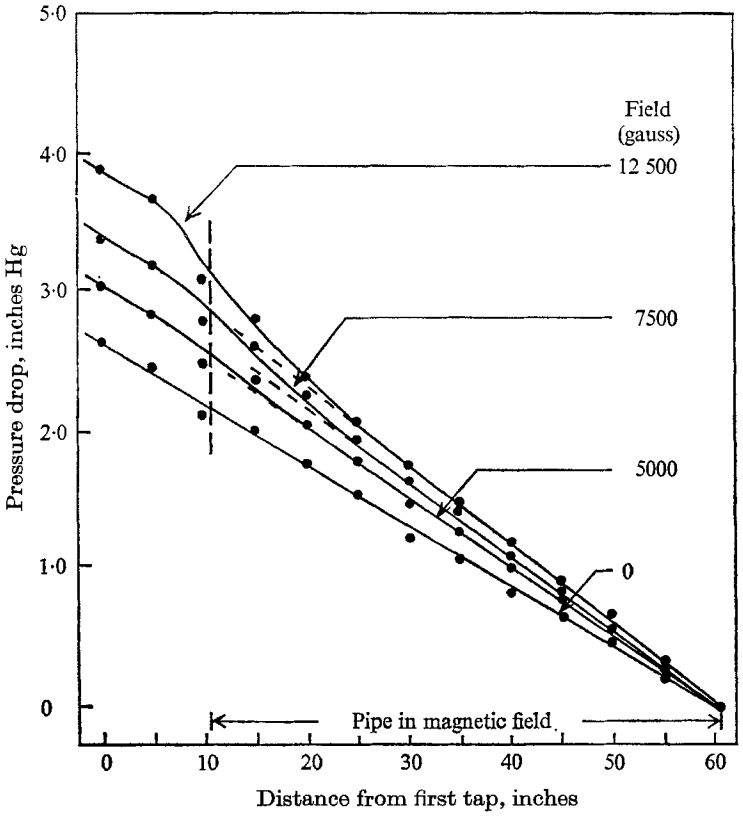

FIGURE 24. Pressure drop data, $Re = 450\,000$.

slightly off the 'laminar line'. This is probably due to the fact that fluctuations may have been present closer to the wall (the probe was located at $r = 0{\cdot}9$) causing some adjustment in the skin friction after the transition point at $r = 0{\cdot}9$ was reached.

Figure 28 shows that the high M/Re data fall along a straight line with a slope about 8 percent higher than the theoretical value of $3\pi/8$ found by Shercliff (1956) for the case of laminar pipe flow in a transverse field. This discrepancy between experiment and theory was also found by several other researchers.†

† Loeffler *et al.* (1969), Khozhainov (1966), Hartmann & Lazarus (1937).

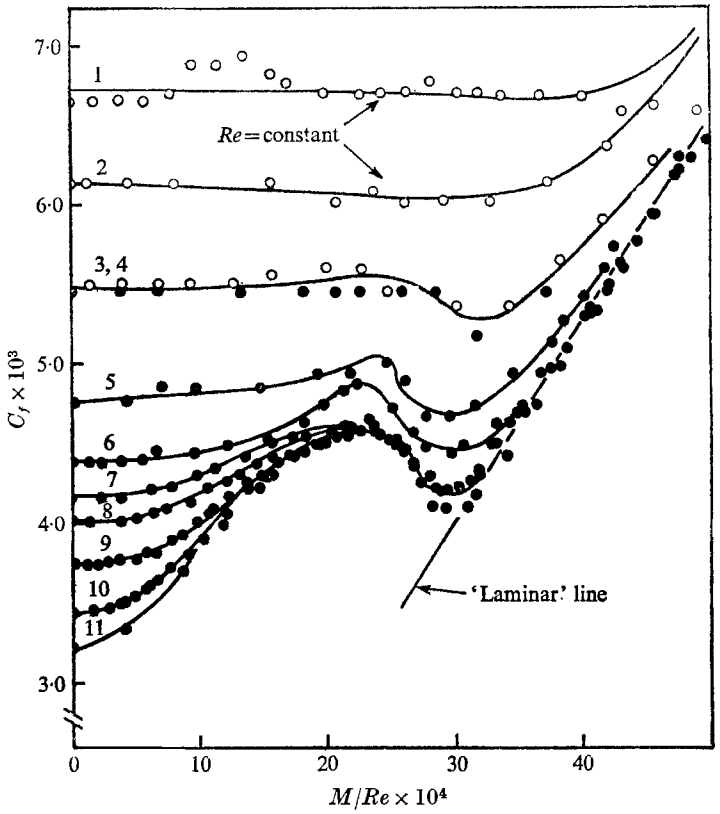

FIGURE 25. MFM skin friction data. ○, pressure transducer data; ●, micromanometer data. Data curve: 1, $Re = 25\,000$; 2, $Re = 35\,000$; 3, 4, $Re = 50\,000$; 5, $Re = 75\,000$; 6, $Re = 100\,000$; 7, $Re = 150\,000$; 8, $Re = 200\,000$; 9, $Re = 300\,000$; 10, $Re = 500\,000$; 11, $Re = 750\,000$.

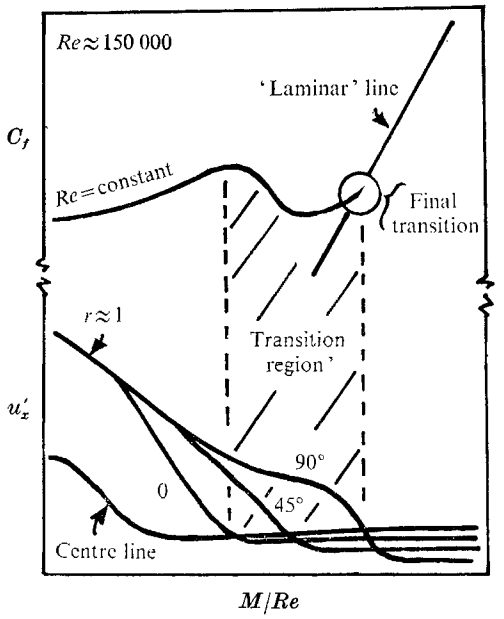

FIGURE 26. Comparison of skin friction and velocity fluctuation data, $Re \approx 150\,000$.

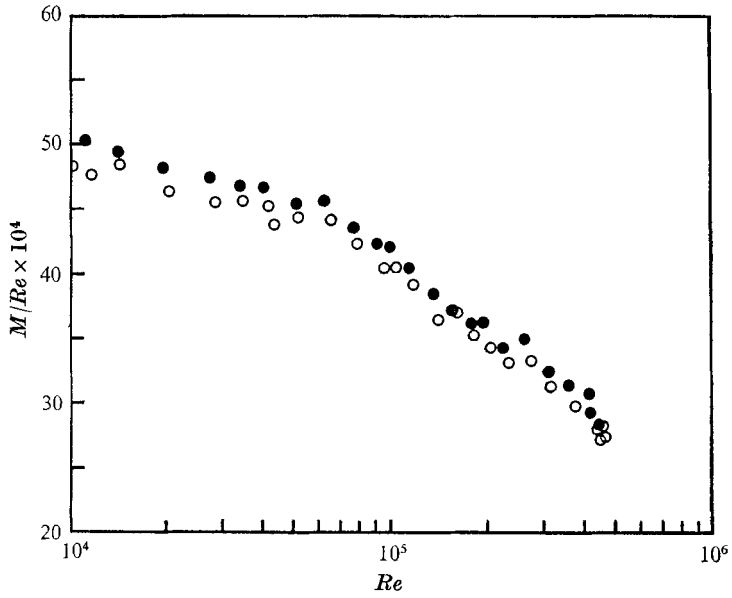

FIGURE 27. Transition data: ●, transition from turbulent to laminar flow; ○, transition from laminar to turbulent flow.

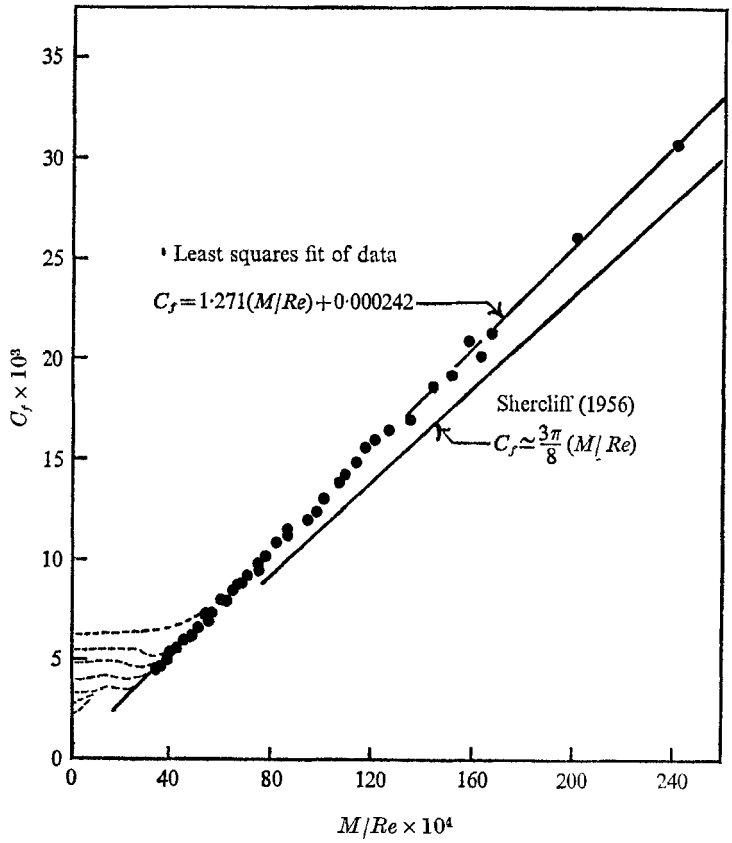

FIGURE 28. Skin friction data for high values of M/Re.

Several factors could cause the slope of the C_f curves to increase: (1) fully developed laminar MFM flow was not attained because of a lack of enough entrance diameters under the field, (2) turbulence from upstream and downstream of the magnet acted as a source of fluctuations which was not damped out, (3) as suggested by Branover (1967) roughness would tend to increase the shear at the wall as it does for the case of no magnetic field.

Although all three of the above could contribute to the increase in slope, our data implicate the incomplete turbulence suppression as the significant factor. Figures 12 and 13 show that 10 and 20 percent of the turbulence remains at $Re = 16000$ and 157000, respectively. There was also a trend in the high M/Re skin friction data for the higher Reynolds numbers to have a slightly higher slope. The residual turbulence must be acting to increase the gradient of the velocity profile on the wall region at 90° from the field. Hence, the average shear stress, $\bar{\tau}_w$, will be higher causing the C_f data to fall above the theoretical 'laminar line'.

The dip in the MFM skin friction data also occurs in data taken in rectangular channels as was shown recently by Hua (1968). Previous experiments in MFM channels did not detect this phenomenon.† The explanation given here for the dip in the pipe C_f data should hold for the channel data also, indicating that even a large aspect ratio rectangular channel exhibits three-dimensional effects in the transition region.

6. Summary and conclusions

The present work consisted of an experimental investigation of isothermal, turbulent, magneto-fluid-mechanic pipe flow in a transverse magnetic field.

And experimental magneto-fluid-mechanic loop was constructed in which a $1\frac{1}{2}$ inch electrically insulated circular test section was suspended horizontally between the pole faces of a large d.c. electromagnet. (The flow was fully established turbulent flow before it entered the magnetic field.) A d.c. magnet was used that could create fields up to 13000 gauss with pole faces 12 in. by 50 in. and a gap of 3 in. Measurements of local quantities in the flow were made with a traversing mechanism located at the exit of the test section. Skin friction, velocity profile, turbulence intensity profile, and velocity fluctuation spectra data were presented which quantitatively exhibit the Hartmann effect and damping of the velocity fluctuations for a broad range of magnetic fields and flow rates. Skin friction measurements were made as a function of the magnetic field in a Reynolds number range from 25000 to 750000. Local parameters (such as mean velocity profiles and velocity fluctuations profiles) were measured for Reynolds numbers from 16000 to 157000.

A qualitative study of the influence of the magnetic field on the velocity fluctuations was made in order to gain insight into the character of the flow. It was found that the fluctuations are damped out strongly in the neighbourhood of the centre of the flow and then, as the magnetic field is increased, an angular dependence appears. The fluctuations near the wall, at 90° from the field, are the last ones to be damped. It was also observed that these last fluctuations have an

† Murgatroyd (1953), Brouillette & Lykoudis (1967).

intermittent character at the lower Reynolds numbers. A further increase in the field damped out these last fluctuations and the turbulence intensity decreased to a 'laminar' level. Velocity fluctuation intensity profiles confirmed the above picture with quantitative data. When the fluctuations near the wall (where they are maximum) begin to be damped out the flow enters the 'transition' régime. The velocity profiles are making their final adjustment and the skin friction is in the 'dip' region. The damping of the centre-line velocity fluctuations (for small fields) was found to follow an exponential of the form:

$$\exp(-0{\cdot}54M^2/Re^{0{\cdot}75}).$$

As the field was increased the constant in the above exponential form changed when the angular dependence appeared in the flow near the wall.

Velocity profiles along a diameter 0° from the field flattened as the field was increased (Hartmann effect) and along 90° the profiles became more rounded than the zero-field profile. These effects are due to the fact that the ponderomotive force decelerates the flow in the central portion and accelerates the flow near the wall at 0°, but not at 90°.

Measurements of the one-dimensional Taylor power spectrum of the axial velocity fluctuations indicated that the magnetic field damped the amplitude of all frequencies. The normalized spectrum showed a weak tendency to shift to higher frequencies for small fields and then to the lower frequencies after 'transition' occurred. The bulk of the fluctuation energy was found in the low frequency range, (0 to 200 c/s) and for $Re = 52000$ and 157000 an inertial subrange was apparent at the higher frequencies for which the spectrum $F(n) \approx n^{-\frac{5}{3}}$.

Axial pressure gradient data indicated that the magnetic entrance effect on the axial pressure drop was limited to a few diameters except for high Reynolds numbers and high fields. The two taps that were just before the entrance into the field always indicated the slope of the zero field data. Following the short magnetic entrance, the axial pressure drop was linear for the rest of the test section to the exit. Two taps in this linear portion were chosen and the complete set of skin friction data were taken.

The existence of the dip in the skin friction data (plotted against the ratio of the Hartmann number to Reynolds number, M/Re), first observed by Loeffler *et al.* (1969), was confirmed. This dip was explained from the data of the present experiment as the region in which the transition from turbulent to a 'laminar' flow takes place. The flow is then a mixed flow: along a 0° diameter the fluctuations are damped out, whereas, along a 90° diameter, the fluctuations are still present. When all of the fluctuations are damped out, the skin friction takes a value on the 'laminar' line. The dip is somewhat analogous to the well-known dip in the zero field skin friction data (plotted against the Reynolds number) that occurs in the transition region at about $Re = 2300$.

The skillful construction of various parts of the experimental apparatus by J. Ayres, R. Conner, and R. Carlson is gratefully acknowledged.

The authors are grateful to the National Science Foundation for support under Grant GK-181.

REFERENCES

BLUM, E. A., ZAKYA, M. V., EUANOV, Y. E. & MICHAILOV, U. A. 1967 *Heat and Mass Transfer in Magnetic Fields.* (In Russian.) Riga.

BRANOVER, H. 1967 *Magnitnaya Gidrodinamika*, **4**, 3.

BRANOVER, H. & LIELAUSIS, O. 1965 *Sov. Phys.-Tech. Phys.* **10**, 2.

BRANOVER, H., SLYUSAREV, N. & SHCHERBININ, E. 1965 *Magnitnaya Gidrodinamika*, **1**, 1.

BROUILLETTE, E. & LYKOUDIS, P. 1967 *Phys. Fluids*, **10**, 995.

FARADAY, M. 1832 *Phil. Trans.* 175.

FRAIM, F. & HEISER, W. 1968 *J. Fluid Mech.* **13**, 397.

GARDNER, R. A. 1969 Ph.D. Thesis, Purdue University, Lafayette, Indiana, U.S.A.

GARDNER, R. A. & LYKOUDIS, P. S. 1971 *J. Fluid Mech.* (In the Press.)

HARTMANN, J. & LAZARUS, F. 1937*a* *Danske Videnskab. Selskab. Mat.-Fys. Medd.* **15**, 6.

HARTMANN, J. & LAZARUS, F. 1937*b* *Danske Videnskab. Selskab. Mat.-Fys. Medd.* **15**, 7.

HUA, H. 1968 Ph.D. Thesis, Purdue University, Lafayette, Indiana, U.S.A.

IHARA, S., TAJIMA, K. & MATSUSHIMA, A. 1967 *J. Appl. Mech.* **34**, 3.

KHOZHAINOV, A. 1966 *Sov. Phys.-Tech. Phys.* **11**, 2.

LAUFER, J. 1951 *NACA Report* 1053.

LOEFFLER, A., MACIULAITIS, A. & HOFF, M. 1969 *Phys. Fluids*, **12**, 2445.

MURGATROYD, W. 1953 *Phil. Mag.* **44**, 1348.

PAPAILIOU, D. & LYKOUDIS, P. S. 1968 *Int. J. Heat Mass Trans.* **11**, 1385.

SAJBEN, M. & FAY, J. 1967 *J. Fluid Mech.* **27**, 81.

SHERCLIFF, J. 1956 *J. Fluid Mech.* **1**, 644.